RESEARCH PAPER

Elucidation of Degradants in Acidic Peak of Cation Exchange Chromatography in an IgG1 Monoclonal Antibody Formed on Long-Term Storage in a Liquid Formulation

Sejal Gandhi • Da Ren • Gang Xiao • Pavel Bondarenko • Christopher Sloey • Margaret Speed Ricci • Sampathkumar Krishnan

ABSTRACT

Purpose An IgG1 therapeutic monoclonal antibody showed an increase in acidic or pre-peak by cation exchange chromatography (CEX) at elevated temperatures, though stable at 2–8°C long-term storage in a liquid formulation. Characterization effort was undertaken to elucidate the degradants in CEX pre-peak and effect on biological activity.
Methods Purified CEX fractions were collected and analyzed by peptide mapping, size exclusion, intact and reduced-alkylated reversed phase techniques. Biophysical characterization, isoelectric focusing and Isoquant analysis were also performed to determine nature of degradants. Bioassay and surface plasmon resonance experiments were performed to determine the impact on biological activity of the degradants.
Results No major degradation due to oxidation, clipping or aggregation was detected; conformational differences between purified fractions observed were not significant. Sialic acid, N-terminal glutamine cyclization and glycation differences contributed to the CEX pre-peak in the mAb control sample; increase in CEX pre-peak at 25°C and higher was caused by additive degradation pathways of deamidation, related isomerization and clipping.
Conclusions The observed CEX pre-peak increase was caused by multiple degradations, especially deamidation and clipping. This elucidation of degradants in CEX peaks may apply to other therapeutic IgG1 monoclonal antibodies.

ABBREVIATIONS

Asn	asparagine
Asp	aspartic acid
bis-ANS	4,4′-dianilino-1,1′-binapthyl-5,5′-disulfonic acid dipotassium salt
CD	circular dichroism
CDR	complementarity-determining region
CEX	cation exchange chromatography
cIEF	capillary isoelectric focusing
FcRn	neonatal Fc receptor
FTIR	Fourier transform infrared spectroscopy
HIC	hydrophobic interaction chromatography
HPLC	high performance liquid chromatography
IgG1	immunoglobulin gamma 1
mAb	monoclonal antibody
PIMT	protein L-isoaspartyl methyltransferase
RP	reversed-phase
SAH	S-adenosyl homocysteine
SEC	size exclusion chromatography
SPR	surface plasmon resonance
TFF	tangential flow filtration

S. Gandhi · D. Ren · G. Xiao · P. Bondarenko · C. Sloey · M. S. Ricci · S. Krishnan
Formulation and Analytical Resources
Process and Product Development, Amgen Inc.
Thousand Oaks, California 91320, USA

S. Krishnan (✉)
Amgen Inc.
One Amgen Center Drive, MS: 8-1-C
Thousand Oaks, California 91320, USA
e-mail: skrishna@amgen.com

Springer

INTRODUCTION

Proteins are susceptible to various covalent modifications that may result in structural and functional changes (1–5). Cation exchange chromatography (CEX) is widely used in biopharmaceutical industry to monitor charge heterogeneity in proteins and separate protein variants including deamidated species (6–10). However, characterization of the peaks separated by CEX is an analytical challenge due to the complexity of the nature of charge heterogeneity associated with recombinant monoclonal antibodies (mAbs). Characterization of charge heterogeneity, therefore, requires a systematic and detailed analysis using orthogonal techniques. Some of the common modifications that can be detected by CEX are formation of disulfide bonds, N-terminal pyroglutamate cyclization, C-terminal lysine processing, deamidation, isomerization, glycosylation and oxidation (1,11).

Deamidation and isomerization are common post-translational modifications occurring in proteins that can cause heterogeneity. Previous research has established the effects of protein sequence and conformation, buffer type, pH, and ionic strength on deamidation of asparagine (Asn) residues. Deamidation reaction of Asn is accelerated at high pH and high temperature, whereas isomerization of aspartic acid (Asp) is more common at acidic pH close to pH 5 and below (12–16). It is important to understand the degradant profile under these different solution conditions during development of protein therapeutics to determine if the molecule will be stable during manufacturing, shipping, long-term storage and administration to patients. The kinetics of deamidation and isomerization reactions have been investigated extensively using synthesized peptides and small proteins (17–21). Glycine and serine are known to be the most destabilizing amino acids in $N+1$ position for Asn deamidation and isomerization (21–23). Furthermore, deamidation of Asn residues can cause loss in potency (24,25). Yan *et al.* have shown that deamidation of Asn55 in the complementarity determining region (CDR) leads to a decrease in ligand binding activity and loss in potency due to intermediate succinimide formation (24). Therefore, it is important to characterize and monitor these modifications and develop formulation strategies to minimize their formation if deemed as critical product quality attributes.

Identification of deamidation using conventional analytical techniques can be complicated, especially in large protein molecules, such as mAbs. Previously, Paranandi *et al.* described the utility of enzymatic methylation for characterizing sites of deamidation in a large protein (26). Capillary zone electrophoresis (CZE) is another technique that has been employed to separate isoAsp, Asp, and Asn forms in human growth hormone-releasing factor (27). In spite of the recent advancements, detection of deamidation in mAbs still remains a challenging task. Traditionally, peptide mapping coupled with mass spectrometry (MS) is used to identify the reaction sites of deamidation or isomerization in a large number of protein molecules. However, the deamidated and isomerized residues are not always discernible due to the mass shifts of 1 and 0, respectively, as was found in the current work. Therefore, it is still difficult to achieve definitive identification and complete accounting of those reaction sites on large molecules. In addition, unless the digested peptides containing the modified residues are separated from the corresponding original peptides on the peptide maps, the reaction sites are effectively not detectable. The isoaspartyl form of the peptide typically elutes in front of the aspartyl form using reversed-phase high performance liquid chromatography (RP-HPLC), but base-line resolution of the degradant peaks may not be achieved for larger peptides having a single modification. Another complicating factor is that peptide mapping may itself induce degradation during sample preparation (28,29). A recent technique involving application of $H_2^{18}O$ for identifying the deamidation and isomerization sites on a humanized mAb showed advantages over standard peptide mapping procedure (30), but the approach may not be practical for routine analysis of stability samples.

The recombinant IgG1 mAb used in the current study is produced using Chinese hamster ovary cells, and the molecule is glycosylated. It demonstrated excellent physical and covalent stability in different solution conditions at the recommended storage temperature of 2–8°C using conventional analytical methods including size exclusion chromatography (SEC), RP-HPLC, reduced CE-SDS, and peptide mapping. However, at elevated temperatures of 25°C and higher, a significant increase in CEX acidic peak or pre-peak was observed. The use of such elevated temperatures to accelerate degradation in protein molecule is critical to help monitor manufacturing lot-to-lot variability in stability profile that may not be manifested in samples at 2–8°C storage in a reasonable period of time. Such accelerated conditions also help support recommendation of manufacturing as well as long term storage conditions where exposure to such temperatures is possible resulting in different degradation mechanisms.

This manuscript describes the investigation performed utilizing a battery of bioanalytical, biophysical and biological characterization tools to elucidate degradants in CEX pre-peak of IgG1 formed on long term storage at 25°C. Also, pure CEX peak fractions were collected and characterized to determine if the degradants affect the biological activity of the molecule. In addition, the utility of an improved 30-minute trypsin digestion method (31) to identify degradations in the CEX pre-peak is also discussed.

MATERIALS AND METHODS

Materials

Purified recombinant IgG1 mAb in 10 mM acetate, 5% sorbitol, pH 5.2 was supplied by Amgen process and purification development group at 30 mg/ml. The antibody stock solution was concentrated in a Labscale™ Tangential Flow Filtration (TFF) system (Millipore Corp., Bedford, MA) to a final protein concentration of 70 mg/mL. Polysorbate 20 was added at 0.004% (w/v) before incubating samples at different temperatures. 4,4′-Dianilino-1,1′-binapthyl-5,5′-disulfonic acid dipotassium salt (bis-ANS) was obtained from Sigma (St. Louis, MO). Isoquant® isoaspartate detection kit was from Promega (Madison, WI). All other chemicals used were of reagent grade or higher.

CEX and Collection of Purified Fractions

CEX was developed and optimized to characterize degradation(s) in stability studies during formulation development. A ProPac® WCX-10, 4 mm×250 mm, weak cation exchange column (Dionex Corp., Sunnyvale, CA) was used. The protein was injected to the column over the first 5 min using a 10 mM sodium phosphate buffer at pH 6.8 (mobile phase A) at a flow rate of 1 mL/min. The elution buffer 10 mM sodium phosphate, 250 mM sodium chloride, pH 6.8 (mobile phase B) was initially applied to the column at 15%, and then linearly ramped to 45% over 75 min for a gradient of 1 mM/min elution buffer. After complete protein elution, the column was washed with 10 mM sodium phosphate, 1 M sodium chloride, pH 7.7 (mobile phase C) for 6 min and equilibrated with mobile phase A for 6 min. Absorbance was measured at 215 nm, and the resulting peaks were integrated using Chromeleon HPLC software. Sample load was 20 µg for each injection.

CEX pre-peak, main peak and post-peak fractions were collected using a preparative ProPac® WCX-10 column, 22 mm×250 mm, (Dionex Corp., Sunnyvale, CA) at a flow rate of 5 mL/min on AKTA HPLC (GE Amersham Biosciences, Piscataway, NJ). Ten injections of 100 µL injection volume of 70 mg/mL (7 mg/injection) were made using a degraded sample (25°C, 6 months) that contained ~27% of CEX pre-peak. A gradient method was used for the separation of different species, and multiple peak fractions were collected. Immediately after peak collection, the fractions were dialyzed in formulation buffer (10 mM acetate, 5% sorbitol, pH 5.2) using snakeskin® pleated dialysis tubings with a molecular weight cut-off (MWCO) of 10 kDa (Thermo Scientific, Rockford, IL). The purified fractions were then concentrated to ~10 mg/mL using Amicon 10,000 MWCO centripreps (Millipore Corp., Bedford, MA) followed by sterile filtration with 0.22 µM vacuum filters.

Chromatography Methods

The collected CEX pre-peak, main peak and post-peak fractions were analyzed by SEC, intact mAb RP-HPLC, and reduced and alkylated RP-HPLC techniques to quantify high molecular weight (HMW) aggregates, low molecular weight (LMW) clips and oxidized species, respectively. The error margin for chromatography data was ±5% based on method-induced variability determined from multiple sample analyses. An Agilent 1100 equipped with Chromeleon software was utilized for all chromatography methods.

SEC

This was performed using a TSKgel G3000SWXL column, 7.8 mm×30 cm, 5 µm (TOSOH Bioscience LLC, King of Prussia, PA). The elution was carried out isocratically with 100 mM sodium phosphate, 300 mM sodium chloride, pH 6.8 at a flow rate of 0.6 mL/min. Absorbance was measured at 220 nm. Peak areas in the chromatograms were used to quantify the HMW aggregate species.

Intact mAb RP-HPLC

A Zorbax 300SB C8 column, 2.1 mm×150 mm, packed with 3.5 µm particles was used for intact RP-HPLC method. The mobile phase A was 0.1% trifluoroacetic acid (TFA; J.T. Baker, Phillipsburg, NJ) in water and mobile phase B was 0.1% TFA, 70% isopropanol, 20% acetonitrile, 10% water. The column temperature was maintained at 75°C. A gradient from 10% B to 33% B was run over 30 min followed by a gradient from 33% B to 100% B until 32 min at a flow rate of 0.3 mL/min with detection wavelength of 215 nm. A flush step was performed with 90% B for 10 min.

Reduced and Alkylated RP-HPLC

This method utilized a Pursuit 3 diphenyl 2 mm×250 mm column (Varian, Palo Alto, CA). The mAb samples were diluted to 2 mg/mL in denaturation buffer containing 0.1 M Tris, 7.0 M guanidine, 1.0 M dithiothreitol (DTT), pH 8.3. This was followed by incubation at 65°C for 15 min. Carboxyamidomethylation was achieved by the addition of freshly prepared 1.0 M iodoacetamide (IAM) and 10-minute incubation in the dark at room temperature. Excess IAM was quenched with the addition of 1.0 M DTT. Mobile phase A contained 0.1% TFA in water, and mobile phase B contained 0.1% TFA in acetonitrile. A gradient from 35% B to 41% B was run over 65 min at a flow rate of 0.2 mL/min. The column temperature was maintained at 65°C.

Biophysical Analysis: Intrinsic and Bis-ANS Fluorescence, Fourier Transform Infrared Spectroscopy (FTIR), and Circular Dichroism (CD)

Purified CEX main peak and pre-peak fractions of the IgG1 mAb were analyzed using biophysical techniques to explore the possibility of conformational differences between fractions that could affect the protein binding behavior on ion-exchange column, leading to an increase in CEX pre-peak. All biophysical analyses were carried out at room temperature after the purified CEX fractions were buffer exchanged in formulation buffer at pH 5.2.

Intrinsic fluorescence was monitored at 0.05 mg/mL protein concentration using a Photon Technology International (PTI) spectrofluorometer (Birmingham, NJ) with excitation wavelength of 295 nm. To monitor bis-ANS fluorescence, 0.7 µL of 7.43 mM bis-ANS (Sigma, St. Louis, MO) was spiked in 0.5 mL of 0.5 mg/mL protein. The scan was taken using the PTI spectrofluorometer after equilibration for 5 min with excitation wavelength of 395 nm. In addition, infrared spectra of CEX peak fractions at >8 mg/mL concentration were acquired using a Bomem Prota infrared spectrometer (Quebec City, Canada) utilizing BioTools liquid sampling cell, equipped with CaF_2 windows that provided a 6 µm pathlength. The second-derivative data was analyzed after normalization (32,33). Finally for far-UV analysis, Jasco 810 spectropolarimeter (Easton, MD) was used to collect spectra from 190 to 250 nm range for 0.4 mg/mL mAb formulation.

Capillary Isoelectric Focusing (cIEF)

The charge variants were separated by cIEF using a Beckman neutral coated, 50 µm ID×30 cm long eCAP™ Neutral capillary on a ProteomeLab PA800 (Beckman Coulter Inc., Brea, CA) with a UV detector. An ampholyte mix was prepared by adding one part of pH 8–10.5 ampholine with three parts of pH 3–10 ampholine (GE Healthcare, Piscataway, NJ). The mAb was diluted to 0.3 mg/mL in the ampholyte solution containing the ampholyte mix and 0.2% hydroxypropyl methylcellulose with internal standards at pI 9.5 and pI 7.2. N, N, N′, N′-Tetramethylethylenediamine (TEMED) (Invitrogen Corp., Carlsbad, CA) was added to the sample at 1% *v/v* to prevent the pI 9.5 marker from focusing in the distal end of the capillary. The anolyte buffer was 20 mM phosphoric acid; the catholyte buffer was 40 mM NaOH. Mobilization was achieved using cathodic mobilizer solution (Bio-Rad, Hercules, CA). Elution was monitored at 280 nm. Temperature was maintained at 20°C for the capillary and 10°C for the samples. Separation of the mAb was performed at −25 kV with 8-minute focusing period followed by a 30-minute mobilization step at −25 kV.

Isoquant®

The amount of isoaspartate in the IgG1 mAb test samples was measured using protein L-isoaspartyl methyltransferase (PIMT) enzyme supplied in the Isoquant® isoaspartate detection kit (Promega Corp., Madison, WI). The test samples were diluted to ~10 mg/mL in formulation buffer to correspond with ~70 µM of the mAb. Denaturation was performed using a stock solution of 8 M urea, 0.1 M Tris, pH 7.5 to achieve a final concentration of 4.5 M urea in 50 µL. Samples were subsequently reduced with 250 mM DTT followed by incubation at room temperature for 15 min, and addition of 0.1 M Tris to dilute urea concentration to 4 M. The protocol supplied with the Isoquant kit was followed for further reaction. The S-adenosyl homocysteine (SAH) standard curve was prepared with a range of SAH concentrations, such that 40 µL injection volumes corresponded to 10, 30, 50, 70, and 90 pmols of SAH. HPLC analysis was done using the Synergi™ Hydro-RP column, 150 mm×4.6 mm, 4 µ (Phenomenex, Torrance, CA) with a guard column attached. The mobile phase A was 50 mM potassium phosphate, pH 6.2, and mobile phase B was 100% methanol with detection at 260 nm. The gradient defined in the Promega Isoquant kit protocol was utilized. The isoAsp content was calculated by comparing the peak area of SAH in the test sample with the SAH standard curve.

Lys-C Hydrophobic Interaction Chromatography (Lys-C HIC)

Limited proteolysis was performed by incubating the enzyme Lys-C with mAb samples at an enzyme to protein ratio of 1: 500 for 25 min at pH 7.5. Digestion was stopped with the addition of 10% TFA to lower the pH to 5.0. HIC separation was performed by injecting 100 µg of the digests on Dionex ProPac® HIC-10 column, 4.6 mm×100 mm, with 5 µ particle size and 300Å pore size. The column temperature was maintained at 25°C at a flow rate of 0.8 ml/min. Mobile phase A contained 20 mM sodium phosphate, 1.8 M ammonium sulfate, pH 7.0 and mobile phase B contained 20 mM sodium phosphate, pH 7.0. The gradient was from 25% B to 100% B over 32 min. The UV absorbance was measured at 220 nm.

Tryptic Peptide Mapping Followed by Mass Spectrometry Analysis

An improved 30-minute trypsin digestion method was used to minimize digestion-induced modifications (31). The IgG1 samples were diluted to 1 mg/mL in 0.5 mL of pH 7.5 denaturation buffer (7.5 M guanidine HCl, 0.25 M

Tris). Reduction was accomplished with the addition of 3 µL of 0.5 M DTT followed by 30 min incubation at room temperature. Carboxymethylation was achieved with the addition of 7 µL of 0.5 M iodoacetic acid. The reaction was carried out in the dark for 15 min at room temperature. Excess iodoacetic acid was quenched with the addition of 4 µL of 0.5 M DTT. Reduced and alkylated mAb samples were buffer exchanged with 0.1 M Tris, pH 7.5 digestion buffer using a NAP-5 column (GE Healthcare, Piscataway, NJ). Lyophilized trypsin was dissolved in water to a final concentration of 1 mg/mL. Digestion was started with the addition of 1 mg/mL trypsin solution to the reduced, alkylated, and buffer exchanged samples to achieve a 1:25 enzyme to substrate ratio. Digestion was carried out at 37°C for 30 min. The final digest was quenched with the addition of 5 µL of 20% formic acid. RP separation of tryptic peptides was conducted using an Agilent 1100 series CapLC system (Agilent, Santa Clara, CA), and separation of peptides was achieved with a Polaris ether 3 µm C18 2 mm×250 mm column (Varian, Palo Alto, CA). Mobile phase A contained of 0.1% TFA in water and mobile phase B contained 90% acetonitrile, 9.915% water, 0.085% TFA. The column temperature was maintained at 50°C, and the flow-rate was 0.2 mL/min. A linear gradient from 0 to 50% B was run over 195 min. A Thermo Finnigan (San Jose, CA) LTQ-Orbitrap mass spectrometer was used in-line with the HPLC system to identify the protein digests. A full MS scan followed by three data dependent MS/MS scans were setup to acquire both the mass and the sequence information for the peptide maps. The full scan was collected with a resolution of 30,000 and the MS/MS scans were acquired with a resolution of 15,000 in the Orbitrap. The spray voltage was 5 kV and the capillary temperature was 300°C. The instrument was tuned using the doubly charged ion of a synthetic peptide, fibrinopeptide B. The MS/MS spectra were obtained using a normalized collision energy of 35%. Mass Analyzer software developed in-house was used for peptide identification (34,35).

The error margins were derived by peptide mapping quantification practice in the lab. Peptide mapping procedure was shortened and optimized to minimize artifacts/errors as previously published (31). A large number of IgG peptide maps were processed in the lab using an automated protocol (36) to define the error margins.

Anti-proliferation Bioassay

The bioassay for the IgG1 mAb was a growth-inhibition assay to detect the biological activity in test samples. Cells from a specific cell-line were incubated with the mAb reference standard, control, and test samples in the presence of a constant concentration of growth factor. Cell inhibition was then measured by incubating the cells with Alamar blue dye. The measured Alamar blue fluorescence was proportional to the amount of viable cells and inversely proportional to the concentration of the mAb. The biological activity of the test sample was determined by comparing the test sample response to that of the reference standard.

Active Antigen Binding Concentration Assay Using Surface Plasmon Resonance (SPR)

Determination of IgG1 mAb binding to antigen (in this case a growth factor receptor) was performed using a Biacore 2000 instrument (GE Healthcare, Piscataway, NJ). Antigen was immobilized on a CM5 sensor chip to a level of 10,000 RU using Amine Immobilization kit (EDC + NHS, quenched with ethanolamine, GE Healthcare, Piscataway, NJ). A blank surface without antigen was prepared in series with immobilized flow cell allowing for automatic blank subtraction. IgG1 mAb samples were diluted to 4.5 µg/mL in HBS-EP buffer (GE Healthcare, Piscataway, NJ) and injected at 5 µL/min over the sensor chip surface for 1 min. Response units after injection were used to calculate active binding concentration using IgG1 mAb standard curve and linear regression analysis. Sensor chip surface was regenerated using a buffer containing 100 mM monobasic potassium phosphate, 500 mM NaCl.

Neonatal Fc Receptor (FcRn) Binding Using SPR

The impact of increase in CEX pre-peak in temperature-incubated samples on pharmacokinetic properties of the IgG1 mAb was determined by analyzing FcRn binding affinity of purified CEX fractions. A Biacore 2000 instrument (GE Healthcare, Piscataway, NJ) was used. Recombinant humanized FcRn was immobilized on a CM5 sensor chip to a level of 200 RU using Amine Immobilization kit (EDC + NHS, quenched with ethanolamine, GE Healthcare, Piscataway, NJ). A blank surface without FcRn was prepared in series with immobilized flow cell allowing for automatic blank subtraction. The test samples were diluted in a buffer containing 50 mM sodium phosphate, 150 mM sodium chloride, 0.01% polysorbate 80, pH 6.0 and injected at a flow rate of 100 µL/min. Following 30s injection (association phase), buffer was allowed to flow over the surface at 100 µL/min for 2 min (dissociation phase). Sensor chip surface was regenerated with Dulbecco's phosphate buffered saline (Sigma-Aldrich, St. Louis, MO). For each test sample, a concentration series was run from 1.64 nM to 1 µM. Data was analyzed using BIAEvaluation software and was fit using the heterogeneous ligand model.

RESULTS

Analysis of Degradation Differences Between Control and Temperature-Incubated Samples

To characterize the nature of the CEX pre-peak species, a variety of analytical techniques were utilized to compare degraded temperature-incubated samples to controls with respect to physical, covalent, and functional aspects of the IgG1 mAb. The duration of temperature incubation for the samples was 6 months at 25°C for all analyses except for cIEF. The samples used for cIEF analysis were incubated for 1 year at 25°C and the results were compared to the corresponding CEX pre-peak data. The control sample was stored at −20°C prior to analyses.

CEX Stability Data

The CEX profile of the IgG1 mAb stored at 25°C over 1 year is shown in Fig. 1. The data show a progressive increase in CEX pre-peak with no significant change in total area of the chromatographic peaks over the time period. The inset in Fig. 1 shows the CEX pre-peak at recommended storage temperature of 4°C and elevated temperature of 25°C until 12 months. The rate of increase in pre-peak was 0.3% per month at 4°C and 2.5% per month at 25°C. This degradation rate was eight-fold higher at 25°C than at the recommended storage temperature of 4°C. Incubation at temperatures higher than 25°C (such as 37°C) further accelerated the CEX pre-peak increase (data not shown).
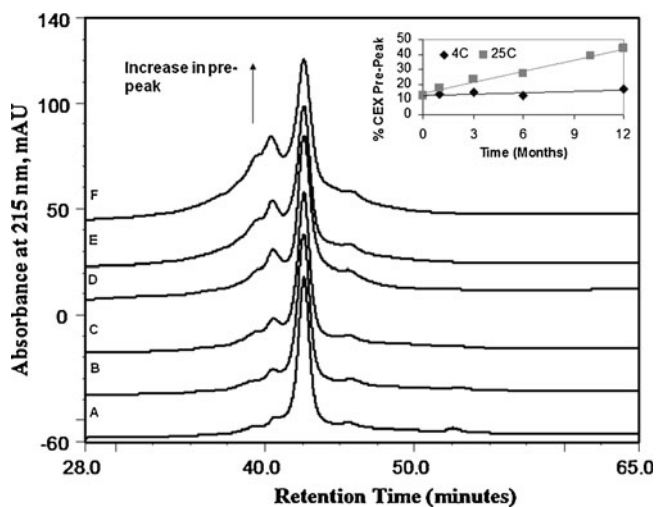
cIEF

cIEF is often used as a complementary analytical tool to CEX in detecting acid charge variants (37). The electropherograms for a 25°C 1-year incubated sample and a control sample are shown in Fig. 2. The 25°C 1-year incubated sample showed an increase of 24.3% in acidic variants with respect to the control sample using cIEF while no major differences were observed in total peak area between the two samples. The CEX pre-peak for the same sample showed 27% increase over the pre-peak of control sample. This clearly showed that the CEX pre-peak increase in the 25°C sample was associated with an increase in acidic variants, and it was not an artifact of the CEX method itself.
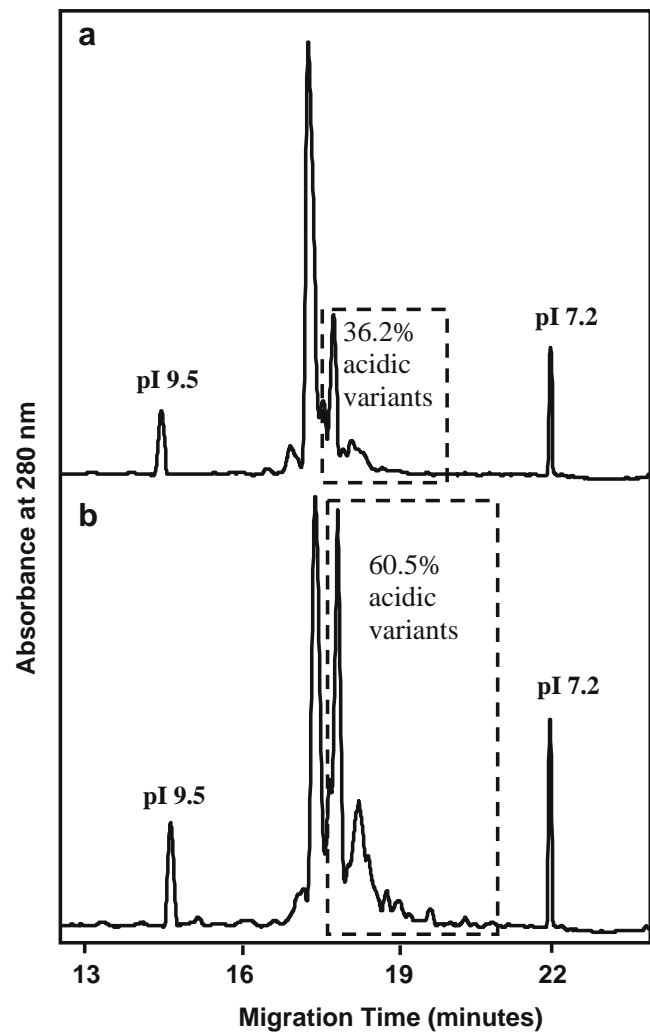

Fig. 1 CEX chromatograms of IgG1 antibody sample stored at 25°C for (*A*) initial time zero, (*B*) 1 month, (*C*) 3 months, (*D*) 6 months, (*E*) 10 months, (*F*) 1 year. A linear increase in CEX pre-peak from 13% at initial time 0 to 44% at 1 year is shown. The inset shows the progressive increase in pre-peak at 4°C and 25°C over 1 year for the same sample.

Fig. 2 cIEF electropherograms of (**a**) IgG1 control sample and (**b**) incubated sample stored at 25°C for 1 year. An increase of 24.3% in acidic variants was observed in the 25°C sample.

Tryptic Peptide Mapping Followed by Mass Spectrometry Analysis

Tryptic peptide mapping was performed on a frozen control sample stored at −20°C and a 6-months 25°C incubated IgG1 mAb sample to identify covalent modifications. The UV overlay of the reversed-phase chromatograms of these two tryptic digests is shown in Fig. 3a. The UV trace was not sensitive enough to detect degradation differences between the control and incubated samples due to the elution of multiple peptides in a single UV peak. The native peptides and their degradation products were therefore identified from their tandem mass spectra. The degradation percentages were calculated based on the intensities of the extracted mass chromatograms of the native peptide and the degraded peptides. Detailed description of this quantitation method can be found in an earlier study (29). Data analysis on the peptide mapping mass spectrometry data revealed that the temperature-incubated sample had more degradation products compared to the control sample. These degradation products

were observed on four amino acid residues in the heavy chain of the IgG1 molecule: Gln1, Asn59 and/or Asn61, Asp282, and Asn386 (Table I). No significant degradation was observed in the light chain. About 96.7% of the N-terminal glutamine residue was converted to pyro-glutamic acid in the control sample. After incubation at 25°C for 6 months, the conversion rate on Gln1 was 99.2%. Even though no deamidation product was observed on Asn386 in the control sample, 2.2% deamidation product was found on Asn386 containing peptide in the incubated sample as shown in Fig. 3b. All the above modifications lead to a charge change of −1 on the IgG1 molecule, which can cause an increase of CEX pre-peak. In addition to N-terminal glutamine cyclization and deamidation, isomerization was also found in the incubated IgG1 sample. No isomerization product was detected on the heavy chain Asp282 residue in the control sample, but 1.0% of this Asp residue was converted to isoAsp in the incubated sample.

Peptide mapping was performed on samples after reduction of the disulfide bonds and percentage of modified amino acid residues on light or heavy chain was calculated

Fig. 3 (**a**) Overlay of tryptic digest RP chromatograms of the control sample (*blue*) and 6-months 25°C incubated sample (*red*). The *arrows from left to right* show isoAsp386, Asn386, and Asp386 peaks. (**b**) Zoomed in region of (**a**). It shows an overlay of RP chromatograms of Asn386 modification to Asp386 and iso-Asp386 in the control sample (*blue*) and 6-months 25°C sample (*red*).
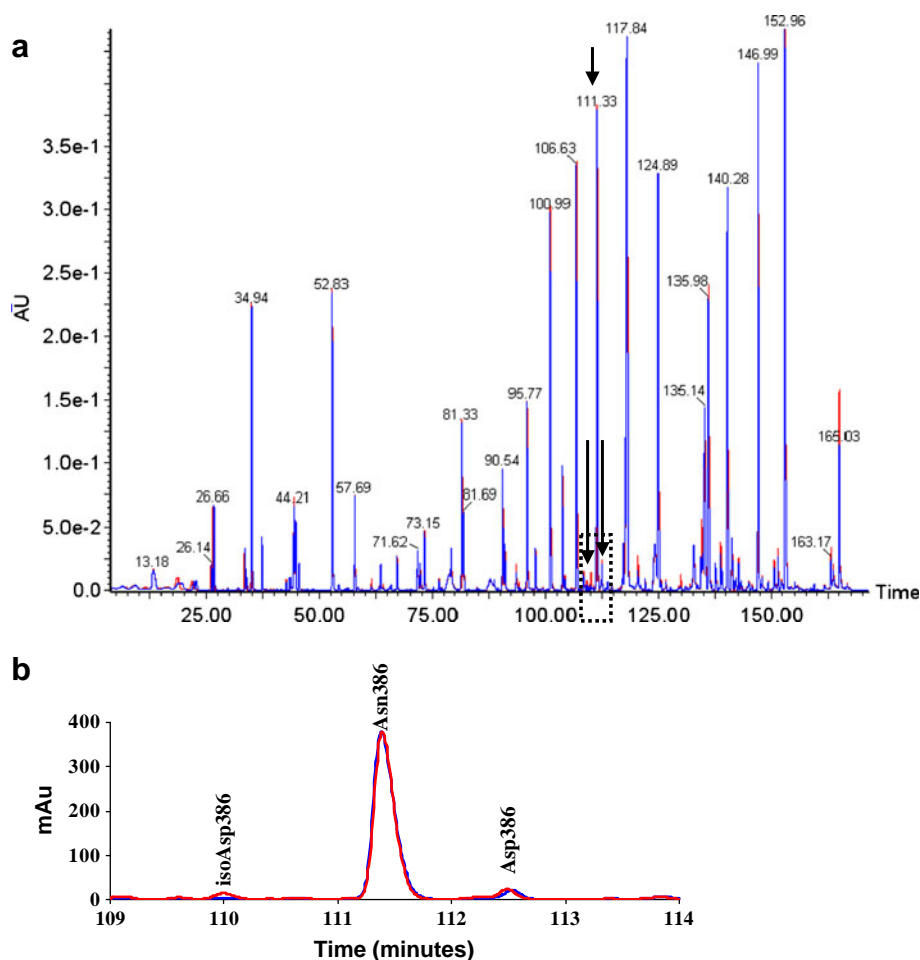
Table I Summary of Covalent Modification Changes Between the Frozen Control Sample Stored at −20°C and a 6-Months 25°C Incubated Sample of the IgG1 mAb

Modifications	% Modification in control sample	% Modification in incubated sample	% Difference	Net charge change
HC: Q1 to pyroE1	96.7 ± 0.5	99.2 ± 0.5	2.5	−1
HC: Asn59 and/or Asn61 to Asp and isoAsp	0.4 ± 0.2	0.5 ± 0.2	0.1[a]	−1
HC: Asp282 to isoAsp282	0	1.0 ± 0.2	1.0	0
HC: Asn386 to Asp386 and isoAsp386	0	2.2 ± 0.5	2.2	−1
Total			5.8	

[a] Value within experimental error

on molar basis. IgG antibodies have two identical halves, each including one light and one heavy chain. Modification events on the different halves of the same intact IgG molecule are statistically independent (38). Modification of any residue results in three populations of intact IgG molecules containing none, one and both residues modified, linked by the following equation:

$$(PrM + PrU)(PrM + PrU) = PrM^2 + 2(PrM)(PrU) + PrU^2$$

where Pr—probability; M—modified residue; U—unmodified residue; M^2—both residues modified; U^2—both residues unmodified.

Therefore, the total degradation was calculated using the above equation to account for degradation in both chains. Since the charge-related degradation contributed to 4.8% for one half of the mAb, this corresponded to 9% charge-related degradation in the intact IgG1 mAb using the above equation. Similarly, the total degradation in the incubated sample identified by peptide mapping was 5.8% for one half corresponding to 11% degradation in the intact IgG1 mAb.

Isoquant®

To explore the possible contribution of isomerization to CEX pre-peak increase, the IgG1 mAb 6-months 25°C incubated sample was analyzed by Isoquant® method. The SAH content in the incubated sample was determined by fitting the peak area in the standard linear regression plot (inset in Fig. 4). Since the injected protein concentration was known, the percent isoAsp in the incubated test sample was determined. The SAH peak area in the 6-months 25°C incubated sample was significantly higher than in the control sample (Fig. 4). The increase in isoAsp in incubated sample with respect to the frozen control was 7.4%. Peptide mapping identified isomerization of only one Asp residue, Asp282, in the heavy chain. It constituted no more than about 1% of the total isoAsp detected by Isoquant. The increase in isoAsp detected by Isoquant is therefore likely to be related to deamidation of Asn to Asp (and isoAsp) followed by isomerization of Asp in the incubated sample.

Anti-proliferation Bioassay and Antigen Binding Assay by SPR

The functionality of the degraded mAb was assessed to determine if the material with increased CEX pre-peak had compromised potency. The relative potency of 6-months incubated samples at 4°C, 25°C and 37°C from bioassay and Biacore antigen binding experiments are shown in Table II. There were no significant changes in relative potency by cell proliferation assay or antigen binding measured by Biacore for the incubated sample stored at 25°C for 6 months, even though the CEX pre-peak increased to 30.6% at 25°C over the same time period as compared to 17.2% pre-peak at 4°C. The relative potency increased to 153% for the sample incubated at 37°C for 6 months and containing 62% CEX pre-peak. Based on orthogonal investigations, it was observed that the increase in relative potency at 37°C condition is due to the effect of increased amount of aggregates eluting in CEX post-peak and not due to increase in CEX pre-peak. The linear correlation between increased potency and aggregates was observed from other studies using cell-based bioassay and not discussed here since it is outside the scope of the current work. Antigen binding by an SPR-based active binding concentration assay showed a decrease by relatively small amount to
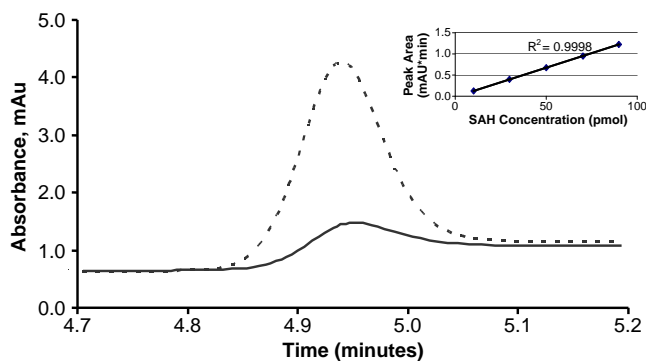

Fig. 4 Isoquant® chromatogram overlay of IgG1 control sample (*solid line*) and sample stored at 25°C for 6 months (*dashed line*). The inset shows the SAH standard curve that was used to calculate SAH content in the test samples.

Table II Summary of the CEX Pre-Peak Data from 6-Months Incubated Samples at Different Temperatures and Corresponding Anti-proliferation Bioassay-Based Potency and Biacore-Based Antigen Binding Results

Sample	% CEX Pre-peak	% Relative potency (n = 3)	% Antigen binding (n = 3)
4°C, 6 months	17.2 ± 0.9	112.4 ± 4.3	103.6 ± 2.0
25°C, 6 months	30.6 ± 1.5	131.2 ± 3.0	105.8 ± 1.8
37°C, 6 months	62.5 ± 3.1	153.4 ± 2.4	92.7 ± 1.2

93%. The enriched CEX pre-peak therefore had no adverse impact on receptor binding and biological activity.

Analysis of Degradations of Collected CEX Fractions

In order to confirm that the attributes of the degraded material can be related to the increased CEX pre-peak, CEX fractions were collected from a degraded sample of IgG1 mAb incubated for 6 months at 25°C, as described in the "Materials and Methods" section. This specific degradation condition and time point was chosen to populate a significant amount of CEX pre-peak. Enriched samples were characterized using a battery of orthogonal analytical techniques, as discussed in this section.

Chromatographic Analysis

Purity of the collected CEX fractions was determined by re-injecting on CEX column (Fig. 5). The purities of the three fractions were 82% for pre-peak, 100% for main peak and 89% for post-peak fraction. In addition, there was no redistribution of the purified main peak fraction on re-injecting on the CEX column, indicating that the CEX pre-peak was not an artifact of chromatography and that the fractions were stable.
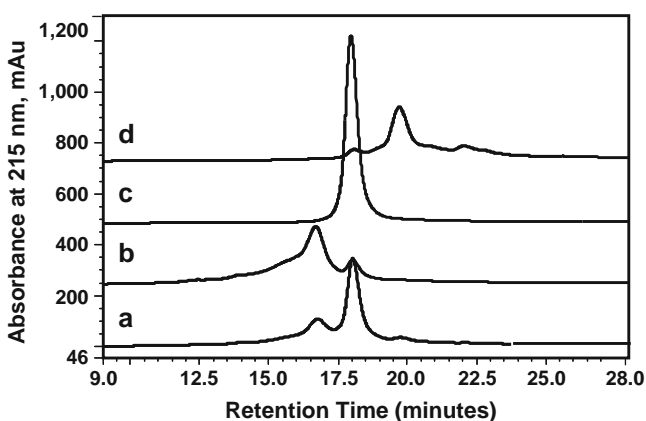

Fig. 5 CEX chromatogram profiles of (**a**) intact IgG1 mAb sample incubated at 25°C for 6 months used for CEX peaks fraction collection, (**b**) purified CEX pre-peak fraction, (**c**) purified CEX main peak fraction, (**d**) purified CEX post-peak fraction. Note that the peak areas are comparable and the difference in peak heights is due to the difference in peak shape.

The collected CEX peak fractions of the IgG1 mAb were analyzed for different degradants by various analytical techniques including SEC, intact mAb RP-HPLC, and reduced and alkylated RP-HPLC techniques. The percentage of the degradant peak area relative to the total peak area by chromatographic analysis was determined and the results are summarized in Table III. The data showed distribution of clips to be 3.5 times more in the CEX pre-peak than in the CEX main peak fraction by intact mAb RP-HPLC. Aggregate species determined by SEC eluted predominantly in the CEX post-peak fraction. Reduced and alkylated RP-HPLC showed enrichment of oxidized species in the CEX post-peak fraction compared to the CEX pre-peak and main peak fractions.

The analysis of CEX fractions by chromatographic techniques indicated that the clips species eluted mainly in the CEX pre-peak fraction (~2.1%) *versus* 0.6% clips in the main peak. Also, 1.7% clip species eluted in the post-peak fraction. The major degradation in the pre-peak fraction relative to the main peak fraction was therefore clipping. However, clips constituted only a small percentage of the CEX pre-peak, indicating occurrence of some other degradant(s) co-eluting within the CEX pre-peak.

Biophysical Analysis

Intrinsic and bis-ANS fluorescence, FTIR and CD techniques were used to investigate potential conformational differences. No major differences in the tertiary structure were observed by intrinsic and bis-ANS fluorescence of the CEX fractions. In addition, FTIR second derivative and

Table III Distribution of LMW Clips, HMW Aggregates, and Oxidized Species in Purified CEX Fractions as Determined by Orthogonal Chromatographic Techniques. There is 3.5 Times More Distribution of Clips in the Pre-Peak Fraction Relative to the Main Peak Fraction. The Error Margin for Chromatographic Techniques Based on Method-Induced Variability is ±5% as Determined from Multiple Sample Analyses

Fraction	% LMW clips	% HMW aggregate	% Oxidation
Intact	2.2 ± 0.1	2.0 ± 0.1	10.1 ± 0.5
Pre-Peak	2.1 ± 0.1	0.3 ± 0.02	9.6 ± 0.5
Main Peak	0.6 ± 0.03	0.2 ± 0.01	7.5 ± 0.3
Post-Peak	1.7 ± 0.09	11.2 ± 0.6	19.5 ± 1.0

far-UV CD spectra indicated comparable secondary structure for the CEX fractions (biophysical data shown in Supplementary Material Fig. S1).

cIEF

The CEX pre-peak fraction of the incubated 6-months 25°C sample consisted mainly of acidic charged variants as shown in electropherograms in Fig. 6. Although cIEF is not capable of identifying the degradants that cause the increase in acidic variants, the data confirmed that the increase in CEX pre-peak in incubated samples was mainly due to degradation reactions that lead to increased acidic charged variants.

Lys-C HIC

There were no significant differences in Lys-C HIC peak profiles between CEX pre-peak and main peak fractions (data not shown due to lack of differences). Isomerized species typically elute earlier in HIC. There were no new early-eluting peaks in the pre-peak fraction relative to the main peak fraction that would have indicated isomerization in CEX pre-peak. This suggested that isomerization was not a significant degradation in the pre-peak fraction and therefore did not notably contribute to the increase in CEX pre-peak in temperature-incubated samples.

Tryptic Peptide Mapping Followed by Mass Spectrometry Analysis

Conventional peptide mapping using 18-hour trypsin digestion at 37°C did not detect significant differences in covalent degradation between the CEX pre-peak and main
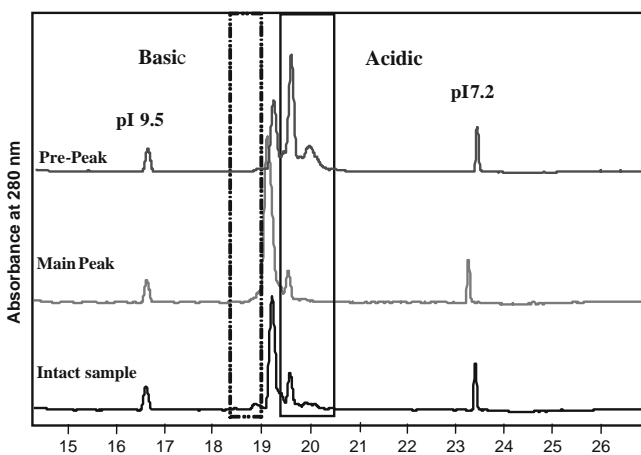

Fig. 6 cIEF electropherogram overlay of a control intact sample, purified CEX main peak fraction, and purified CEX pre-peak fraction. The solid box represents acidic variants, and the dashed box represents basic variants.

peak fractions (data not shown). It is generally known that longer digestion times can induce degradations in proteins. An improved tryptic digestion method (described in the "Materials and Methods" section) using shorter 30-minute trypsin digestion at 37°C was therefore used to detect differences in covalent degradation between the purified CEX pre-peak and main peak fractions (31). The improved peptide mapping method revealed 6% difference in deamidation between purified pre-peak and main peak fractions (Table IV). This corresponded to approximately 11% difference in deamidation in the intact molecule using the statistic described earlier. The heavy chain Asn386 residue, which is known to deamidate rapidly, showed the highest deamidation. The extracted ion chromatograms and MS/MS spectra of Asn386 deamidation are shown in Fig. 7a, b. The 11% difference in deamidation between purified pre-peak and main peak fractions correlated closely with the observed 14% increase in CEX pre-peak over 6 months of incubation at 25°C. The additional 3% pre-peak may be attributed to the formation of LMW clip species observed using intact mAb RP-HPLC and small amounts of oxidized species (Table III).

In addition, some interesting differences in glycation and glycosylation were noted between the purified pre-peak and main peak fractions (Table V). There was about 10.5% glycation and glycosylation difference between the pre-peak and main peak fractions. Non-enzymatic protein glycation products are typically formed by a Schiff's base reaction between the aldehyde groups of reducing sugars and primary amines of proteins. For the IgG1 mAb used in this study, the glucose sugar moiety was found to be attached to the heavy chain amino acid K74 to form a glycation product. Also, glycosylation variants observed were at Asn 297 residue. These differences were not attributed to long-term temperature stress stability in the incubated sample, but rather to the distribution of sugar residues inherent to the mAb. It is to be noted here that CEX was not only able to separate acidic charge variants, but sugar-related charge changes as well.

Anti-proliferation Bioassay

The biological activity (or relative potency) of the purified CEX fractions was determined using cell proliferation method, as discussed earlier. The relative potency of the CEX pre-peak fraction was slightly lower (76%±12%) as compared to the main peak fraction (96%±2%). Though the relative potency of the pre-peak fraction was 76%± 12%, the intact sample retained its biological activity at 114%±2%. The fact that the intact sample retained essentially full biological activity alleviated some of the concerns about the therapeutic impact of increase in degradant in CEX pre-peak. The relative potency of the post-peak fraction was 193±39%. The high relative

Table IV Summary of Deamidation Covalent Modification Changes Between CEX Pre-Peak and Main Peak Fractions Observed Using Peptide Mapping

Modifications	% Modification in CEX main peak	% Modification in CEX pre peak	% Difference	Net charge change
HC: Asn59 and/or Asn61 to Asp and isoAsp	0.2 ± 0.2	0.8 ± 0.2	0.6	-1
HC: Asn386 to Asp386 and isoAsp386	0	5.4 ± 0.5	5.4	-1
Total:			6.0	

potency of the post-peak fraction was due to its predominant constitution of aggregates as discussed previously.

FcRn Binding Using SPR

The CEX pre-peak and main peak fractions were comparable in kinetic (k_{on} and k_{off}) and dissociation constants (K_d) as shown in Table VI. The model used to fit the FcRn: IgG1 binding data included factors to account for binding of IgG1 to a heterogeneous immobilized FcRn population (39). An overlay of one binding curve sensorgram from each pre-peak, main peak, and post-peak fraction is shown in Fig. 8. The pre-peak and main peak sensorgrams were very similar, while the post-peak showed a very different binding profile with a much slower off rate. Post-peak bound with higher apparent affinity to FcRn, likely due to avidity effects of aggregates. This has been observed in past experiments with mAb samples known to contain higher levels of aggregate.

Comparable FcRn binding for CEX pre-peak and main peak fractions indicates that the pharmacokinetic properties and half-life of the IgG1 mAb are likely not impacted by the increase in CEX pre-peak in 25°C temperature-incubated samples.

DISCUSSION

The IgG1 described in this paper displayed a confounding stability profile by CEX. Under normal storage conditions, the mAb did not show a significant increase in CEX pre-peak at 4°C over 1 year of storage. However, a linear increase of nearly 30% in CEX pre-peak was observed at 25°C over the same time period at a rate of 2.5% increase per month. The identity of the degradant was unknown and the mechanism of degradation was elusive. cIEF results also showed an increase in acidic variants in the incubated sample that correlated with the increase in CEX pre-peak. This confirmed that the increase in pre-peak by CEX was not an artifact of chromatography. The purpose of current investigation was, therefore, to characterize the CEX peaks and elucidate the degradation reaction(s) resulting in increase of CEX pre-peak at elevated temperatures over long term storage.

Chromatographic analysis of the collected CEX fractions helped determine that there was no major redistribution of the CEX fractions when reinjected on CEX column. The HMW aggregates eluted exclusively within the CEX post-peak, clips eluted mostly within the CEX pre-peak (relative to the main peak), and oxidized species eluted mostly in the post-peak as shown in Table III. The pre-peak increase was not due to secondary or tertiary structural changes as determined using biophysical techniques, namely intrinsic and bis-ANS fluorescence, FTIR and far UV CD spectral analysis (as shown in Supplementary Material Fig. S1). Also, it was not an artifact of chromatography as confirmed by orthogonal cIEF method. In addition, the role of disulfide variants causing the observed CEX pre-peak increase was investigated by refolding of the IgG1 mAb and no such contributions were detected (data not shown). These results necessitated further investigation of the degradation in CEX pre-peak.

Isomerization reaction especially for hinge peptide residues was investigated as a potential cause for the observed CEX pre-peak increase for the model IgG1 mAb at 25°C and higher temperature. Although isomerization of aspartic or glutamic acid residues does not directly result in generation of charged species, it could indirectly affect surface charge distribution by inducing local conformational perturbation resulting in solvent exposure of neighboring residues Hambly *et al.* have shown isomerization of Asp223 in the hinge region to be the fastest degradation in another IgG1 (40). They pointed that hinge tryptic peptide $SCD_{223}K$ is a polar peptide that elutes early in the void volume in reduced-alkylated reversed phase chromatogram in alkylated form (iodo-acetic acid alkylation, +58 Da), and therefore difficult to detect. In the current study, the $SCD_{223}K$ hinge peptide was identified using the improved 30-minute tryptic digestion method, but no increase in isomerization of Asp223 was detected in the temperature-incubated samples. HIC used commonly in the detection of isomerization (41), coupled with Lys-C limited proteolysis (42) was performed on purified CEX pre-peak and main peak fractions to detect isomerization related differences. However, there was no significant difference in peak profiles of the pre-peak and main peak fractions. Peptide mapping analysis showed only

Fig. 7 **A** Extracted ion chromatograms of Asn386 modification in peptide G$_{373}$FYPSDIAVE-WESN$_{386}$GQPENNYK$_{394}$ in CEX main peak and pre-peak fractions. **B** MS/MS spectra of peptide G$_{373}$FYPSDIAVEWESN$_{386}$GQ-PENNYK$_{394}$ variants are shown. The b and y ions are labeled on top of the fragment ions. N stands for asparagine, D stands for aspartic acid, isoD stands for iso-aspartic acid.
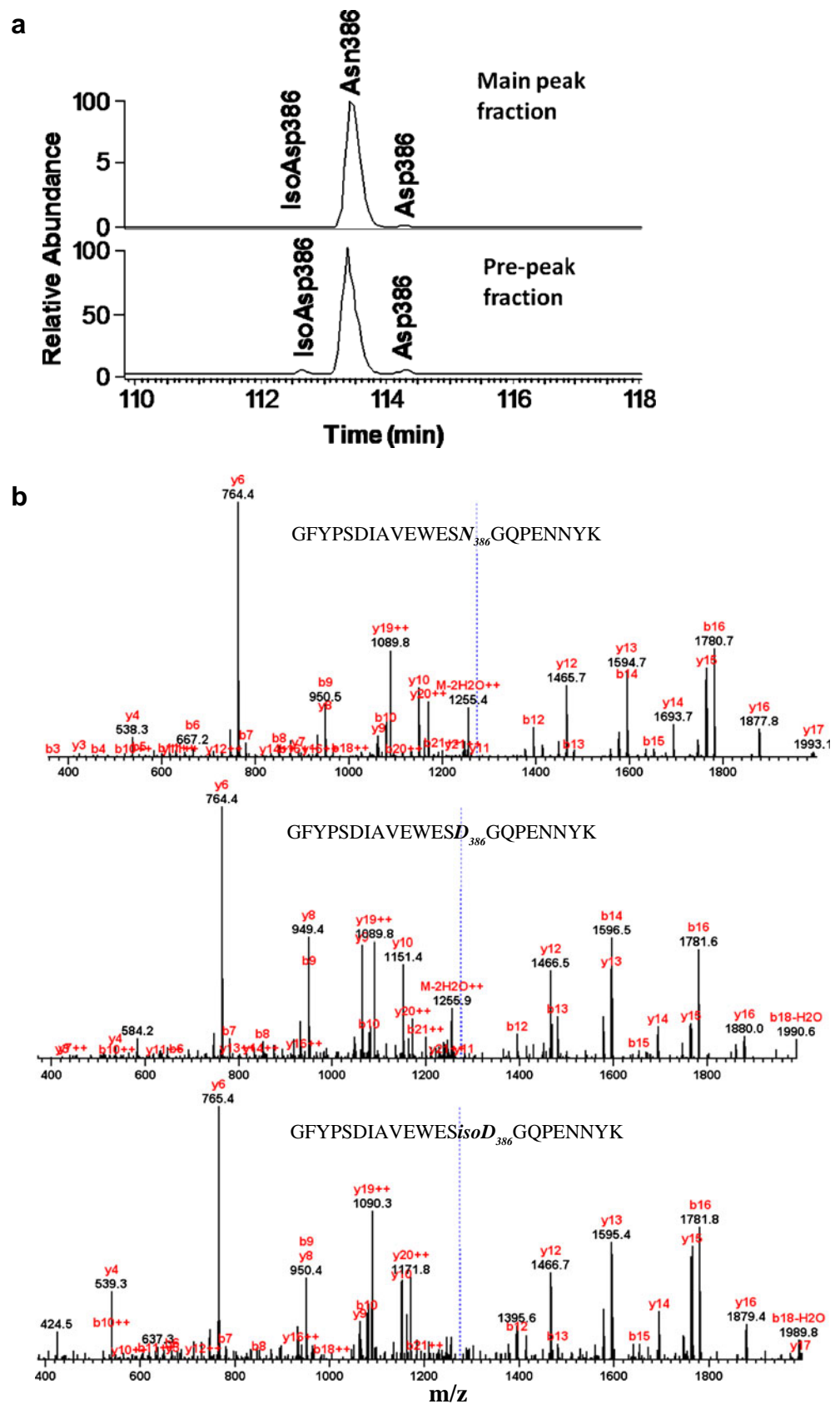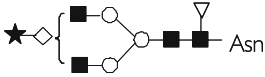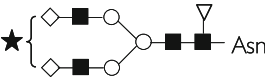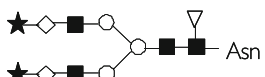
Table V Summary of Glycation and Glycosylation Differences Between the CEX Pre-Peak and Main Peak Fractions Observed Using Peptide Mapping Inherent to the Molecule Due to Process Conditions and Not Caused by Temperature Incubation. Glycosylation Variants are at Asn297 Residue

Glycation and glycosylation variations	% CEX main peak	% CEX pre-peak	% Difference	Net charge change	
HC: K74 Glycation	2.0 ± 0.2	5.3 ± 0.5	3.3	−1	
(glycan structure)—Asn	0.1 ± 0.2	0.8 ± 0.2	0.7	−1	Distribution of glycosylation variations in CEX pre- and main peaks
(glycan structure)—Asn	0.3 ± 0.2	4.8 ± 0.5	4.5	−1	
(glycan structure)—Asn	0.0	2.0 ± 0.5	2.0	−2	
Total			10.5		

★—Sialic acid

◇—Galactose

■—N-acetylglucosamine

○—Mannose

▽—Fucose

1% isomerization of Asp282 residue in the heavy chain compared to nearly 7% isoAsp detected in the incubated sample using Isoquant method. The increase in isoAsp over 6-months for 25°C incubated sample detected by Isoquant was therefore mainly related to deamidation of Asn residue followed by isomerization to isoAsp.

Forced deamidation conditions of the IgG1 mAb showed substantial increase in CEX pre-peak and acidic variants by cIEF providing additional evidence that the increase in CEX pre-peak in elevated temperature-incubated samples may be related to deamidation (data not shown). The improved peptide mapping method with shorter 30-minute trypsin digestion results showed a difference of 11% in deamidation between CEX pre-peak and main peak fractions, mainly in heavy chain Asn386. This correlated closely with the 14% increase in CEX pre-peak observed for the intact incubated sample used for fraction collection. Peptide mapping results also demonstrated more charged glycated and glycosylated forms in CEX pre-peak fraction relative to the main peak fraction. The glycated and glycosylated forms contributed to CEX pre-peak in the control sample and were not related to heat stress in the temperature-incubated sample. Though separation of glycosylated species by CEX has been reported widely in

Table VI Kinetic (k_{on} and k_{off}) and Dissociation (K_d) Constants of CEX Pre-Peak and Main Peak Fractions Using IgG1: FcRn SPR Assay

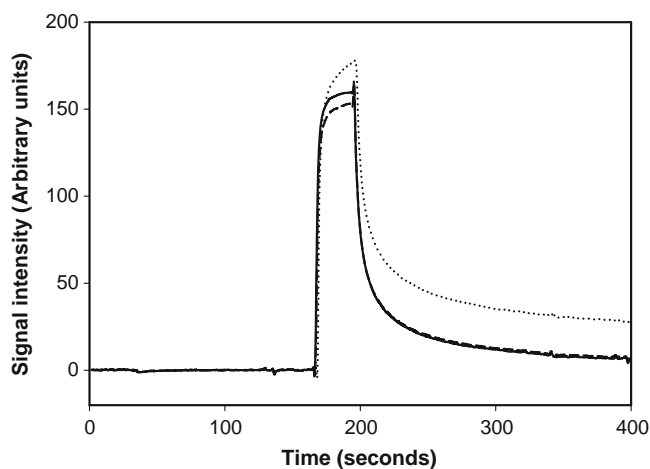| Sample	k_{on1} (1/M*s)	k_{on2} (1/M*s)	k_{off1} (1/s)	k_{off2} (1/s)	K_{d1} (M)	K_{d2} (M)
Pre-Peak	8.01E+05	2.57E+06	0.147	1.00E-02	1.84E-07	3.89E-09
Main Peak	8.13E+05	3.14E+06	0.149	9.85E-03	1.83E-07	3.14E-09

Fig. 8 SPR sensorgrams of CEX main peak (*solid line*), pre-peak (*dashed line*) and post-peak (*dotted line*) fractions. The pre-peak and main peak fractions have comparable FcRn binding profiles; post-peak fraction has higher FcRn binding possibly due to avidity effects of aggregates in the fraction.

literature, there are only a few instances of glycation separation reported for recombinant mAbs. Recently, Quan *et al.* also showed that the acidic peak of CEX was enriched in glycated species in comparison with the main peak for an IgG1 recombinant mAb (43).

Deamidation is considered as a molecular clock for degradation and cause for protein ageing (44–46). Also, deamidation in protein therapeutics can often lead to loss of activity and altered susceptibilities to proteolysis, and can potentially trigger autoimmune responses (24,25,47). We identified deamidation and clipping to be the predominant degradations in the CEX pre-peak of the IgG1 mAb using orthogonal analytical techniques. However, no significant difference in relative potency was observed between temperature-incubated and control samples indicating that deamidation in the temperature-incubated sample did not lead to a loss in potency. The purified CEX pre-peak did show a minor decrease in potency probably due to increase in clip species relative to the control sample. Since deamidation of Asn386 in Fc region was identified as the major degradant in CEX pre-peak, the effect of Fc deamidation on pharmacokinetic properties of the mAb was determined by analyzing FcRn binding using SPR. It is well-known that FcRn has a protective role in regulating the level of circulating IgG and increasing half-life (48,49). Analysis of FcRn binding is therefore a good indicator of pharmacokinetic properties of the IgG1 mAb. The analysis indicated that the CEX pre-peak binds to FcRn with comparable affinity and kinetic properties relative to CEX main peak suggesting that the increase in CEX pre-peak in temperature-incubated IgG1 samples did not have a significant effect on FcRn binding properties. CEX post-peak bound to FcRn with higher apparent affinity, likely due to avidity effects involving dimer and multimer aggregates.

Deamidation of Asn residue has been shown to cause charge heterogeneity of mAbs due to the introduction of one negative charge especially at basic pH and accelerated temperatures. The acidic species that is generated elutes earlier on CEX chromatograms and also migrates faster on cIEF. However, identification of deamidation in mAbs is still a challenge. Deamidation of Asn can also often be confused with isomerization of Asp residue since the end product of both degradations is isoAsp. In large proteins though, the ratio between deamidation end products, isoAsp and Asp can be shifted towards Asp due to conformational constraints (50). It is critical to employ appropriate analytical techniques and modify or enhance methods as needed to identify covalent degradations as utilizing peptide mapping alone has its own challenges due to method-induced degradation (28,29). A battery of orthogonal analytical techniques may be needed to identify and well-characterize degradations, especially deamidation and isomerization, which can be difficult to identify especially due to structural complexity in antibodies.

A key outcome of this characterization work is to demonstrate the physical, chemical, and biological attributes of the CEX pre-peak. Our investigation using multiple orthogonal analytical techniques clearly show that (1) sialic acid, N-terminal glutamine cyclization and glycation differences inherent to the molecule due to process conditions contribute to CEX acidic variants observed in the control sample of the mAb, and (2) the increase in CEX acidic peak at 25°C and above is caused by additive degradation pathways of deamidation and related isomerization reaction as well as LMW clip species. Our findings clearly elucidate the nature of the degradants causing the CEX acidic peak increase for an IgG1 molecule and may be applicable to other IgG1s in general for which similar CEX pre-peak increase has been observed.

ACKNOWLEDGMENTS & DISCLOSURES

REFERENCES

1. Liu H, Gaza-Bulseco G, Faldu D, Chumsae C, Sun J. Heterogeneity of monoclonal antibodies. J Pharm Sci. 2007;97:2426–47.
2. Wang W. Instability, stabilization, and formulation of liquid protein pharmaceuticals. Int J Pharm. 1999;185:129–88.

3. Manning MC, Patel K, Borchardt R. Stability of protein pharmaceuticals. Pharm Res. 1989;6:903–18.

4. Liu D. Deamidation: a source of microheterogeneity in pharmaceutical proteins. Trends Biotechnol. 1992;10:364–9.

5. Aswad D, Paranandi M, Schuter B. Isoaspartate in peptides and proteins: formation, significance, and analysis. J Pharm Biomed Anal. 2000;21:1129–36.

6. Johnson K, Paisley-Flango K, Tangarone B, Porter T, Rouse J. Cation exchange-HPLC and mass spectrometry reveal C-terminal amidation of an IgG1 heavy chain. Anal Biochem. 2006;360:75–83.

7. Perkins M, Theiler R, Lunte S, Jeschke M. Determination of the origin of charge heterogeneity in a murine monoclonal antibody. Pharm Res. 2000;17:1110–7.

8. Weitzhandler M, Farnan D, Rohrer J, Avdalovic N. Protein variant separations using cation exchange chromatography on grafted, polymeric stationary phases. Proteomics. 2001;1:179–85.

9. Weitzhandler M, Farnan D, Horwath J, Rohrer J, Slingsby R, Avdalovic N, et al. Protein variant separations by cation-exchange chromatography on tentacle-type polymeric stationary phases. J Chromatogr A. 1998;828:365–72.

10. Harris RJ, Kabakoff B, Macchi FD, Shen FJ, Kwong M, Andya JD, et al. Identification of multiple sources of charge heterogeneity in a recombinant antibody. J Chromatogr B. 2001;752:233–45.

11. Vlasak J, Ionescu R. Heterogeneity of monoclonal antibodies revealed by charge-sensitive methods. Curr Pharm Biotechnol. 2008;9:468–81.

12. Wakankar A, Borchardt R. Formulation considerations for proteins susceptible to asparagine deamidation and aspartate isomerization. J Pharm Sci. 2006;95:2321–36.

13. Capasso S, Mazzarella L, Sica F, Zagari A, Salvadori S. Kinetics and mechanism of succinimide ring formation in the deamidation process of asparagine residues. J Chem Soc, Perkin Trans. 1993;2:679–82.

14. Patel K, Borchardt R. Chemical pathways of peptide degradation. III. Effect of primary sequence on the pathways of deamidation of asparaginyl residues in hexapeptides. Pharm Res. 1990;7:787–93.

15. Oliyai C, Borchardt R. Chemical pathways of peptide degradation. IV. Pathways, kinetics, and mechanism of degradation of an aspartyl residue in a model hexapeptide. Pharm Res. 1993;10:95–102.

16. Song Y, Schowen R, Borchardt R, Topp E. Effect of 'pH' on the rate of asparagine deamidation in polymeric formulations: 'pH'-rate profile. J Pharm Sci. 2001;90:141–56.

17. Geiger T, Clarke S. Deamidation, isomerization, and racemization at asparaginyl and aspartyl residues in peptides. Succinimide-linked reactions that contribute to protein degradation. J Biol Chem. 1987;262:785–94.

18. Patel K, Borchardt RT. Chemical pathways of peptide degradation: II. Kinetics of deamidation of an asparaginyl residue in a model hexapeptide. Pharm Res. 1990;7:703–11.

19. Kosky AA, Razzaq UO, Treuheit MJ, Brems DN. The effects of α-helix on the stability of Asn residues: deamidation rates in peptides of varying helicity. Protein Sci. 1999;8:2519–23.

20. Robinson NE, Robinson AB. Prediction of protein deamidation rates from primary and three-dimensional structure. Proc Natl Acad Sci USA. 2001;98:4367–72.

21. Capasso S. Estimation of the deamidation rate of asparagine side chains. J Pept Res. 2000;55:224–9.

22. Oliyai C, Borchardt R. Chemical pathways of peptide degradation. VI. Effect of the primary sequence on the pathways of degradation of aspartyl residues in model hexapeptides. Pharm Res. 1994;11:751–8.

23. Li B, Gorman E, Moore K, Williams T, Schowen R, Topp E, et al. Effects of acidic N+1 residues on asparagine deamidation rates in solution and in the solid state. J Pharm Sci. 2005;94:666–75.

24. Yan B, Steen S, Hambly D, Valliere-Douglass J, Bos T, Smallwood S, et al. Succinimide formation at Asn 55 in the complementarity determining region of a recombinant monoclonal antibody IgG1 heavy chain. J Pharm Sci. 2009;98:3509–21.

25. Zhang Y, Martinez T, Woodruff B, Goetze A, Bailey R, Pettit D, et al. Hydrophobic interaction chromatography of soluble interleukin I receptor type II to reveal chemical degradations resulting in loss of potency. Anal Chem. 2008;80:7022–8.

26. Paranandi M, Guzzetta A, Hancock W, Aswad D. Deamidation and isoaspartate formations during in vitro aging of recombinant tissue plasminogen activator. J Biol Chem. 1994;269:243–53.

27. Stevenson C, Anderegg R, Borchardt R. Comparison of separation and detection techniques for human growth hormone releasing factor (hGRF) and the products from deamidation. J Pharm Biomed Anal. 1993;11:367–73.

28. Bongers J, Cummings J, Ebert M, Federici M, Gledhill L, Gulati D, et al. Validation of a peptide mapping method for a therapeutic monoclonal antibody: what could we possibly learn about a method we have run 100 times? J Pharm Biomed Anal. 2000;21:1099–128.

29. Chelius D, Rehder D, Bondarenko P. Identification and characterization of deamidation sites in the conserved regions of human immunoglobulin gamma antibodies. Anal Chem. 2005;77:6004–11.

30. Terashima I, Koga A, Nagai H. Identification of deamidation and isomerization sites on pharmaceutical recombinant antibody using $H_2^{18}O$. Anal Biochem. 2007;368:49–60.

31. Ren D, Pipes GD, Liu D, Shih L, Nichols AC, Treuheit MJ, et al. An improved trypsin digestion method minimizes digestion-induced modifications on proteins. Anal Biochem. 2009;393:12–21.

32. Dong A, Caughey WS. Infrared methods for study of hemoglobin reactions and structures. Meth Enzymol. 1994;232:139–75.

33. Kendrick BS, Dong A, Allison SD, Manning MC, Carpenter JF. Quantitation of the area of overlap between second-derivative amide I infrared spectra to determine the structural similarity of a protein in different states. J Pharm Sci. 1996;85:155–8.

34. Zhang Z. Prediction of low-energy collision-induced dissociation spectra of peptides. Anal Chem. 2004;76:3908–22.

35. Zhang Z. De novo peptide sequencing based on a divide-and-conquer algorithm and peptide tandem spectrum simulation. Anal Chem. 2004;76:6374–83.

36. Zhang Z. Large-scale identification and modification of covalent modifications on therapeutic proteins. Anal Chem. 2009;81:8354–64.

37. Mario N, Baudin B, Aussel C, Giboudeau J. Capillary isoelectric focusing and high-performance cation-exchange chromatography compared for qualitative and quantitative analysis of hemoglobin variants. Clin Chem. 1997;43:2137–42.

38. Rehder DS, Chelius D, McAuley A, Dillon TM, Xiao G, Crousse-Zeineddini J, et al. Isomerization of a single aspartyl residue of anti-epidermal growth factor receptor immunoglobulin gamma 2 antibody highlights the role avidity plays in antibody activity. Biochemistry. 2008;47:2518–30.

39. Martin W, Bjorkman P. Characterization of the 2:1 complex between the class I MHC-related Fc receptor and its Fc ligand in solution. Biochemistry. 1999;38:12639–47.

40. Hambly DM, Banks DD, Scavezze JL, Siska CC, Gadgil HS. Detection and quantitation of IgG 1 hinge aspartate isomerization: the fastest degradation in stressed stability studies. Anal Chem. 2009;81:7454–9.

41. Dick Jr LW, Qiu D, Cheng K. Identification and measurement of isoaspartic acid formation in the complementarity determining

region of a fully human monoclonal antibody. J Chromatogr B. 2009;877:3841–9.

42. Lau H, Pace D, Yan B, McGrath T, Smallwood S, Patel K, *et al.* Investigation of degradation processes in IgG1 monoclonal antibodies by limited proteolysis coupled with weak cation exchange HPLC. J Chromatogr B. 2010;878:868–76.

43. Quan C, Alcala E, Petkovska I, Matthews D, Canova-Davis E, Taticek R, *et al.* A study in glycation of a therapeutic recombinant humanized monoclonal antibody: where it is, how it got there, and how it affects charge-based behavior. Anal Biochem. 2008;373:179–91.

44. Robinson NE, Robinson AB. Molecular clocks. Proc Natl Acad Sci USA. 2001;98:944–9.

45. Reissner KJ, Aswad DW. Deamidation and isoaspartate formation in proteins: unwanted alterations or surreptitious signals? Cell Mol Life Sci. 2003;60:1281–95.

46. Weintraub SJ, Manson SR. Asparagine deamidation: a regulatory hourglass. Mech Ageing Dev. 2004;125:255–7.

47. Vlasak J, Bussat M, Wang S, Wagner-Rousset E, Schaefer M, Klinguer-Hamour C, *et al.* Identification and characterization of asparagine deamidation in the light chain CDR1 of a humanized IgG1 antibody. Anal Biochem. 2009;392:145–54.

48. Yeung YA, Leabman MK, Marvin JS, Qiu J, Adams CW, Lien S, *et al.* Engineering human IgG1 affinity to human neonatal Fc receptor: impact of affinity improvement on pharmacokinetics in primates. J Immunol. 2009;182:7663–71.

49. Israel EJ, Wilsker DF, Hayes KC, Schoenfeld D, Simister NE. Increased clearance pf IgG in mice that lack β_2-microglobulin: possible protective role of FcRn. Immunology. 1996;89:573–8.

50. Capasso S, Di Cerbo P. Kinetic and thermodynamic control of the relative yield of the deamidation of asparagine and isomerization of aspartic acid residues. J Pept Res. 2000;56:382–7.